Search for new physics in the $\mu\mu + e/\mu + \not\!\!E_T$ channel with low-p_T lepton threshold at the Collider Detector at Fermilab

M. Gold and J. Strologas

The CDF Collaboration

August 26, 2008

Abstract

A search for new physics using trilepton data collected with the CDF II detector and corresponding to an integrated luminosity of 976 pb^{-1} is presented. The standard model predicts a low rate of trilepton events while some supersymmetric processes, such as chargino-neutralino production, predict measurable amounts. The $\mu\mu + \ell$ signature is investigated, where ℓ is an electron or a muon, with the additional requirement of large missing transverse energy. In this analysis, the lepton transverse momenta with respect to the beam direction are as low as 5 GeV/c, a selection that improves the sensitivity to new light particles and new particles that result in leptonically decaying taus. At the same time, this low-p_T selection presents additional challenges due to the non-negligible heavy-quark background at low lepton momenta. This background is measured with an innovative technique using experimental data. Several dimuon and trilepton control regions are investigated, and good agreement between the observations and the standard model predictions is observed. In the signal region, we observe one trimuon event and expect 0.4 ± 0.1 $\mu\mu + \ell$ events from standard model processes.

PACS:

1 Introduction

The standard model (SM) of particle physics is enormously successful in describing the known particles and their interactions. However, strong motivation from experimental data as well as important theoretical considerations point to new physics beyond the SM. Astrophysical observations that have resulted in the concordance model of cosmology [1] require a source of dark matter that does not exist in the SM. Theoretically, the SM has well-known limitations in explaining the origin of mass and solving the hierarchy problem. Moreover, it does not satisfy our desire for the unification of the strong and electroweak interactions and the integration of gravity in a unique theory [2].

A powerful strategy for discovering new physics is to search in event topologies where the SM predicts extremely low production rates. One of these topologies is trileptons in hadronic collisions. The lepton candidates we observe at the Tevatron collider result mainly from QCD processes or the decays of massive gauge bosons (W or Z), or photon conversions. The leptons rarely appear in triplets. The trilepton signature is favored by a large class of models of supersymmety (SUSY) [3], in which the lightest supersymmetric particles are the gauginos, the supersymmetric partners of the gauge bosons. The corresponding observable SUSY particles are the charginos ($\tilde{\chi}^{\pm}_{1,2}$) and neutralinos ($\tilde{\chi}^{0}_{1,2,3,4}$), which result from the mixing of the gauginos and the supersymmetric partners of the Higgs bosons, the higgsinos. The associated production of charginos and neutralinos may have a detectable cross section [4] at the Tevatron and may give rise to trilepton events as shown in Figs. 1 and 2. The most common decays are through off-shell vector bosons or sleptons, depending on the gaugino and slepton masses. Under the assumption of R-parity [5] conservation, SUSY particles cannot decay only to SM particles; the lightest SUSY particle (LSP) will be stable and escape detection. Therefore, SUSY events would be characterized by large transverse

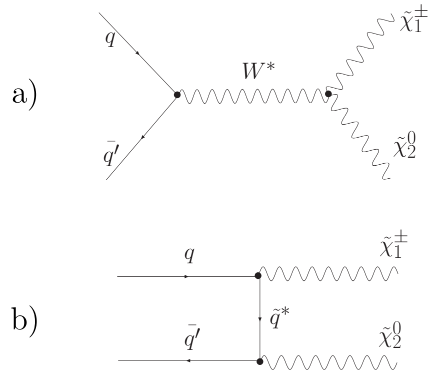

Figure 1: Chargino-neutralino production through a W boson (a) and a squark propagator (b). The latter t-channel is suppressed for scenarios with very massive squarks.

momentum imbalance ("missing transverse energy", or $\not\!\!E_T$). The LSP, which could be the lightest neutralino, is a candidate for the cold dark matter of the universe [6, 7]. In addition, SUSY offers a solution to the hierarchy problem [8, 9, 10] and the possibility for unification of interactions at high energies [11]. The trilepton+$\not\!\!E_T$ topology investigated here is the "golden" signature for the discovery of SUSY at the Tevatron [12, 13, 14, 15, 16].

Searches for non-SM trilepton production have been previously performed by the LEP [17] and Tevatron experiments [18, 19]. In this paper we present a search for new physics with two muons and an additional electron or muon using data collected with the CDF II detector from March 2002 to February 2006 from proton-antiproton collisions at $\sqrt{s} = 1.96$ TeV. The integrated luminosity of our sample is 976 pb^{-1}. To increase the sensitivity to new light particles and tau leptons that decay leptonically, we use a very low p_T threshold (5 GeV/c) for the identified leptons, where p_T is the transverse momentum with respect to the beam direction.

We define several dimuon and trilepton SM-dominated control regions, in which we verify our understanding of the backgrounds. In order to avoid bias, we complete the validation of the background – both in event yields and kinematic shapes – in the control regions before investigating the events in the signal region. Finally, our

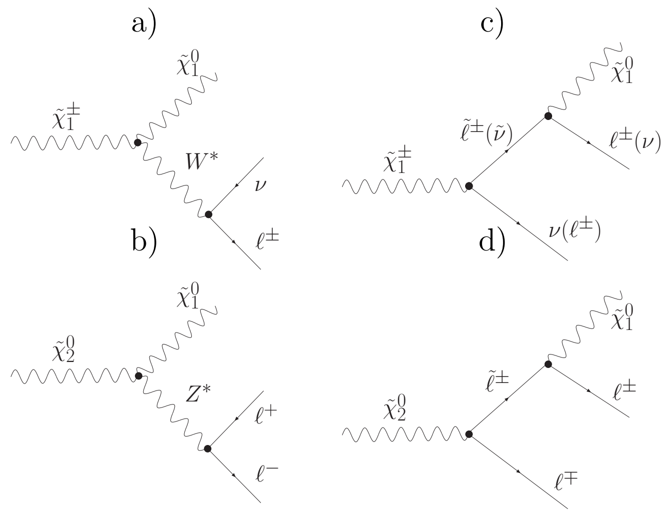

Figure 2: Chargino-neutralino decay through gauge bosons (a,b) and through sleptons (c,d). The branching fractions depend on the masses of the sleptons, which always decay to charged leptons, unlike the gauge bosons. The leptonic signature consists of three leptons in both cases.

result is combined with other trilepton searches at CDF [20] to set a stronger limit on chargino-neutralino production. Although this search is inspired by the SUSY-predicted chargino-neutralino production, the analysis is generic enough to be sensitive to any new physics that would enhance the production of prompt trileptons.

This paper is organized as follows. In Section 2 we describe the CDF II detector. In Section 3 we define the experimental data and Monte Carlo samples, and present an event selection that reduces the SM background expectation while accepting events from possible new-physics signals. Section 4 describes how the SM background rates are estimated, and Section 5 discusses two SUSY model scenarios we consider. In Section 6 we present the determination of the systematic uncertainties on the signal and background event-yield predictions. In Section 7 we present the event yields and kinematic distributions in our control regions that increase the confidence in our understanding of the SM background. Finally, in Section 8 we present the results in the signal region.

2 The CDF II detector

The CDF II detector [21] is a multi-purpose cylindrical detector with projective-tower calorimeter geometry and excellent lepton identification capability. It operates at the Tevatron collider where protons and antiprotons collide with a center-of-mass energy of 1.96 TeV. In our coordinate system the positive z-axis is defined by the proton beam direction and the positive y-axis by the vertical upward direction. The detector is approximately symmetric in the η and ϕ coordinates, where the pseudorapidity η is defined as $\eta = -\ln(\tan(\theta/2))$, θ is the polar angle with respect to $\vec{z}$, and ϕ is the azimuthal angle. We briefly present here the CDF components that are the most critical for this analysis.

In the center of the apparatus, near the beam collision point, a silicon detector of inner radius of 1.35 cm and outer radius of 25.6 cm provides detailed tracking in the $|\eta| < 2$ region, necessary for the accurate determination of the event vertices and impact parameters.

A cylindrical 96-layer open-cell argon-ethane (50%-50%) drift chamber (COT) of inner radius of 44 cm and outer radius of 132 cm provides tracking for charged particles with $\sim$ 100% detection efficiency in the central ($|\eta| < 1.1$) region. The central tracking system is located in a magnetic field of 1.4 T provided by a superconducting solenoidal magnet. The COT tracking momentum relative resolution is $\delta p_T/p_T = 0.0017 p_T (\mathrm{GeV}/c)^{-1}$.

Surrounding the central tracker, and outside the solenoid, a central electromagnetic calorimeter (CEM), composed of layers of lead and scintillator, and a central hadronic calorimeter (CHA), composed of layers of steel and scintillator, measure the energy deposited by traversing electrons, photons and hadrons. The relative energy resolution is $13.5\%/\sqrt{E_T} \oplus 2\%$ for CEM and $75\%/\sqrt{E_T} \oplus 3\%$ for CHA, where the transverse energy $E_T = E\sin\theta$ is quoted in GeV units. A strip chamber (CES), placed inside the electromagnetic calorimeter at the shower maximum position (six radiation lengths), is used for shower shape determination and for matching the calorimeter energy depositions with COT tracks. In the forward region, a plug electromagnetic calorimeter ($1.1 < |\eta| < 2.4$) has a relative resolution of $16\%/\sqrt{E_T} \oplus 0.7\%$ and a plug hadronic calorimeter ($1.3 < |\eta| < 2.4$) a resolution of $130\%/\sqrt{E_T} \oplus 4\%$. The raw missing transverse energy vector is defined as $-(\sum_i \vec{E}_i)_T$, where $\vec{E}_i$ has magnitude equal to the energy deposited in the i^{th} calorimeter tower and direction perpendicular to the beam axis and pointing to that calorimeter tower.

Beyond the calorimeters, the central muon system consists of drift chambers. The central muon chambers (CMU) detect muons in the pseudorapidity range $|\eta| < 0.6$, while the central muon extension (CMX) chambers detect muons in the $0.6 < |\eta| < 1.0$ range, both with a detection efficiency of $\sim 100\%$ for muons above 3 GeV/c. To reduce the hadron punch-through contamination, extra chambers (CMP) are installed outside the CMU chambers, with extra steel absorber added between them. The muons that are detected by both CMU and CMP chambers are called CMUP muons, and their detector signatures cannot be easily caused by hadrons.

The luminosity is measured with Cherenkov counters located close to the beam line at $3.7 < |\eta| < 4.7$.

The CDF trigger system [22] has a three-level pipelined and buffered architecture; each level provides a rate reduction sufficient to allow for processing at the next level with minimal deadtime. The first level consists of special-purpose processors that accept events at rate of 25 kHz, with an average event size of 170 kB, counts main triggering objects and feeds the second level with an event rate of 350 Hz. The second level is also based on hardware and performs a partial event reconstruction, before passing the events to the next level. Finally a software-based third level uses a fast version of the offline event reconstruction to reduce the event rate to 75 Hz, appropriate for writing to tape. The track-based triggers account for approximately 75% of the trigger bandwidth and are used in this analysis. For a muon trigger, the main requirement is that a COT track is geometrically matched to a track segment in a muon detector.

3 The CDF Dataset and signal-region event selection

In order to include in our analysis muons and electrons that come from tau decays, we use a low transverse momentum requirement ($p_T > 5$ GeV/c) for these leptons. For this reason we analyze data collected with the CDF low-p_T dimuon triggers (p_T nominally above 4 GeV/c for both muons). These muons are central in the detector (CMUP or CMX). We measure the trigger efficiency using J/ψ, Υ and Z-boson events collected with single-muon triggers. In these samples, we remove QCD backgrounds using the mass-spectra sidebands, and count the frequency that the non-triggered muon fired the trigger of interest. The plateau value of the trigger efficiency's p_T dependence for single muons is ~ 0.95 and it is reached at $p_T \sim 5$ GeV/c.

After the collected events are processed by the offline reconstruction software, additional requirements are applied for the definition of the dimuon sample. We require that each event has a primary vertex within 60 cm from the nominal center of the detector in the z direction and that at least two muons with transverse momentum above 5 GeV/c originate from that primary vertex and pass the CDF standard muon tracking, calorimetry and track-chamber matching requirements [23]. In events with more than one reconstructed primary vertex, we use the primary vertex that is closest to the tracks of the selected two muons. We specifically require that good-quality COT tracks are geometrically matched with reconstructed track segments in the CMX or CMU+CMP detectors, that the energies deposited in the electromagnetic and hadronic calorimeters are consistent with that expected from minimum ionizing particles, and that the muons are isolated. We define the isolation I as the energy deposited in the calorimeters in a cone of $\Delta R = \sqrt{(\Delta\phi)^2 + (\Delta\eta)^2} = 0.4$ around the muon with the energy associated with the muon subtracted. We require that $I < 0.1 \times p_T c$ if $p_T > 20$ GeV/c or $I < 2$ GeV otherwise. A critical requirement is that the muons are prompt as measured by the impact parameter (d_0), defined as the distance of closest approach of a track to the primary vertex in the transverse plane. We require that $|d_0| < 0.02$ cm if the muon leaves hits in the silicon detector, and that $|d_0| < 0.2$ cm if the muon leaves no hits in the silicon detector. We expect that most muons with large impact parameters come from heavy flavor (bottom- or charm-hadron semileptonic decays), fake muons (light-flavor hadrons such as pions and kaons that decay in flight or punch-through to the muon detectors) and cosmic rays. The heavy flavor (HF) and fake-muon backgrounds dominate at low dimuon masses. Residual cosmic-ray background, not removed by the cosmic filters described in [23], is reduced by requiring that the three-dimensional angular separation ($\Delta\varphi$) of the two highest-p_T muons is less than 178 degrees. After including the selection criteria discussed above, the total muon identification efficiency, as measured with J/ψ and Z boson CDF data, is (90-96)%, rising with increasing muon p_T.

For the trilepton selection, we require the presence of a third muon satisfying the same selection requirements as the first two, or an electron satisfying the CDF standard electron calorimeter, tracking and track-calorimeter matching identification requirements [23]. The transverse energy and momentum of the electron is required to exceed 5 GeV. Tracks associated with electrons should match hits in the CES wires. We require that $I < 0.1 \times E_T$ if $E_T > 20$ GeV or $I < 2$ GeV otherwise, where I is now the energy-based isolation of the electron, and E_T is its transverse energy. Electrons originating from photons that convert into e^+e^- pairs are identified with an algorithm

[23] that seeks nearby tracks with a common vertex and direction. These electrons are removed from the observed data sample. The electron identification efficiency is (75-83)% [23], rising with increasing electron transverse energy, as measured with Drell-Yan electrons.

We define the signal region by the following additional requirements: the dimuon mass (constructed with the two highest-p_T muons) is greater than 15 GeV/c^2, for removal of low-mass resonances, and outside the Z mass window $76 < M_{\mu\mu} < 106$ GeV/c^2. In addition, we require the missing transverse energy ($\not\!\!E_T$) to exceed 15 GeV, in order to select events with undetected new particles while rejecting Drell-Yan, HF, and fake-muon backgrounds. Finally, we require low jet multiplicity ($N_{\rm jet} \leq 1$), where jets with transverse energy above 15 GeV are counted, in order to reduce the $t\bar{t}$ background. In this analysis we use jets defined by a fixed-cone algorithm [23] with a cone size of $\Delta R = 0.4$. We require that jets deposit less than 90% of their measured energy in the electromagnetic calorimeter, in order to avoid counting electrons or photons as jets. Jet energies are corrected [24] to represent better the energy of the final-state hadrons. Global and local corrections are applied as well as inclusion of corrections for the effects of multiple interactions. These corrections are also applied to the raw missing transverse energy for the calculation of $\not\!\!E_T$, which is also corrected for the presence of muons in our events. We check the consistency of the observed data compared to the SM predictions in the control regions that are described in Section 7.

4 Standard Model Backgrounds

To determine the significance of any disagreement between prediction and observation, and also to set limits on production cross sections and masses of new particles, we need a reliable background estimation. The major SM source of dimuons is the Drell-Yan

(DY) process and, in events with low dimuon mass, HF production and the fake-lepton background. In the trilepton regions, the dominant backgrounds are DY (accompanied by a fake lepton), dibosons, and HF. Because HF and fake leptons are difficult to model with Monte Carlo (MC) simulations due to sizable higher-order QCD effects and the imperfect modeling of the leptons' isolation in a high particle-multiplicity hadronic environment, we estimate these backgrounds using CDF data. All other backgrounds are estimated with MC simulation.

4.1 Data-estimated Backgrounds

We first estimate the fake-lepton background, using an independent CDF data sample. Subsequently, we use this fake-lepton background and the MC-estimated DY contribution in our HF-estimation method.

4.1.1 Fake leptons

"Fake" leptons are reconstructed lepton candidates that are either not real leptons or are not prompt and do not originate from semileptonic decays of HF quarks. In the case of muons, the fakes can be light-flavored hadrons, such as pions and kaons or part of hadronic showers, that penetrate ("punch through") the calorimeters and reach the muon detectors or decay to muons in flight. In the case of electrons, fakes are jets that are mis-reconstructed as electrons, often due to neutral pions that decay to photons, which are detected by the electromagnetic calorimeter. We can thus associate the fake leptons with light-flavor partons. Using multijet CDF datasets collected with jet-based triggers, we measure the "fake rate", *i.e.*, the probability for a generic track (jet) to be mis-reconstructed as a muon (electron) and pass our selection criteria. The fake-rate is measured as a function of the track's (jet's) transverse momentum (energy) and pseudorapidity. The fake rate is of the order of 10^{-2} for tracks to be incorrectly reconstructed as muons and increases with the p_T of the muon candidate's track. The fake rate of a jet being reconstructed as an electron is of the order of 10^{-4} and falls with increasing E_T. The fake rates increase for higher rapidity leptons [25].

To determine the muon+fake (i.e., fake dimuon) background, we use single-muon low-p_T-triggered data. For each event, we require one good muon candidate that passes the requirements of our analysis. We then apply the fake rate on all other tracks in the event, except on the track of a second muon (to remove DY contamination of the fake background). We remove events in which the muon+track mass is within the Z boson window ($76 < M_{\mu\mu} < 106$ GeV$/c^2$) and $35 < \not\!\!E_T < 55$ GeV. These events are associated with decays of real Z bosons produced at rest, where one decay muon is not detected, resulting in $\not\!\!E_T$ equal to about half the mass of the Z boson. We investigate the heavy flavor contamination in this light-flavor-dominated background, caused by a real muon coming from a heavy-quark semileptonic decay, which is mis-reconstructed as an isolated track instead of a muon. This contamination is negligible (approximately 0.2% of the background), mainly because of the background-rejection power of our muon isolation requirement. Because the single-muon low-p_T trigger was not always present during data taking, the dimuon fakes extracted using this trigger are normalized to the dimuon CDF data luminosity, in order to represent the size of fake dimuon contamination in our analysis dataset.

For the determination of the dimuon+fake (i.e., fake trilepton) background, we use our dimuon low-p_T-triggered CDF dataset, require two good muons, and model the third fake leptons by applying the fake rate to the extra tracks. We assume that the number of events with two fake leptons is negligible, given the low value of the fake rates. In order not to over-count the trilepton fakes, we require the three leptons in our signal MC and background MC samples to be kinematically matched with the generated ones.

4.1.2 Heavy Flavor

One of the most significant challenges of this analysis is the consideration of muons with transverse momentum as low as 5 GeV/c. This low p_T requirement increases our acceptance, but at the same time contaminates our sample with HF and fake-lepton events.

We present here an innovative technique for the determination of the amount of this background using the observed data. We construct an HF-rich (HFR) dataset by reversing the impact parameter requirement for at least one of the observed muons, so that the absolute value of its impact parameter is above 0.02 cm if there are silicon hits associated with the muon's track, or above 0.2 cm if there are no silicon hits. In both cases, the offline upper $|d_0|$ cut is 0.8 cm. We also require the dimuon mass to be less than 35 GeV/c^2. Monte Carlo studies show that above that value we expect mainly DY and a negligible HF background. We investigated the expected dimuon mass spectrum of DY and fake-lepton in the HFR sample and we determined that the effect of the contamination is negligible.

We subsequently use the HFR dimuon mass shape combined with the absolute fake dimuon mass distribution plus the absolute DY dimuon mass distribution from MC simulation in order to fit the observed data. All data samples other than HFR include the low impact parameter requirement. Because we observe negligible DY in the same-charge dimuon channel, we perform the fit for same-charge and opposite-charge dimuons separately. This helps us validate our HF-estimation method in the HF-rich same-charge dimuon environment. The only free parameter of the fits is the HF normalization – the DY contribution is fixed based on the theoretical cross section and the integrated luminosity of the observed data, and the fake-lepton background distribution is fixed based on the absolute expectation, as described in Section 4.1.1. The results of the fits can be seen in Figs. 3 and 4, for opposite-charge and same-charge muons, respectively. From the two fits, we extract two HF normalization factors that are applied as weights to the original unweighted same-charge and opposite-charge dimuon HFR events, in order to describe the HF background in the observed data. The same weights are used in all kinematic control regions. The weight for the opposite-charge HF dimuons is 1.94 ± 0.04 and for the same-charge HF dimuons is 1.12 ± 0.05, where the uncertainties come from the fits. This tells us that we expect twice as many opposite-charge HF events in the low-impact parameter region compared to the high-impact parameter one. Overall, the ratio of opposite-charge HF to same-charge HF events in the inclusive observed data after the normalization is $\sim$ 4:1, a value that is also verified with $b\bar{b}/c\bar{c}$ MC simulation and is a result of the conserved charge in the underlying quark-pair production and the rates of cascade semileptonic decays of b-hadrons. In regions with no HFR events, we estimate the size of this background by extrapolating the HF prediction from neighboring dimuon control regions that contain sufficient number of events.

The trilepton HF background is estimated by requiring that the normalized HFR sample has a third lepton. If there are no events satisfying this requirement, then we extrapolate from either neighboring dimuon or trilepton control regions with sufficient statistics. For example, we have no HFR data in the trilepton signal region. We estimate the HF background there by extrapolating from the low-$\not\!\!E_T$ region, where we have trilepton HFR events. For the extrapolation we use the dimuon $\not\!\!E_T$ distribution, using the fact the $\not\!\!E_T$ distribution is similar for dimuon and trilepton events. We verify this fact with the use of MC-simulated $b\bar{b}/c\bar{c}$ events.

For the determination of the HF-estimation method systematic uncertainty, we re-estimate the HF background by redefining the HFR dataset using either a requirement on the number of silicon detector hits for the muon that has large impact parameter (at least two silicon hits), and/or applying a requirement on the impact parameter

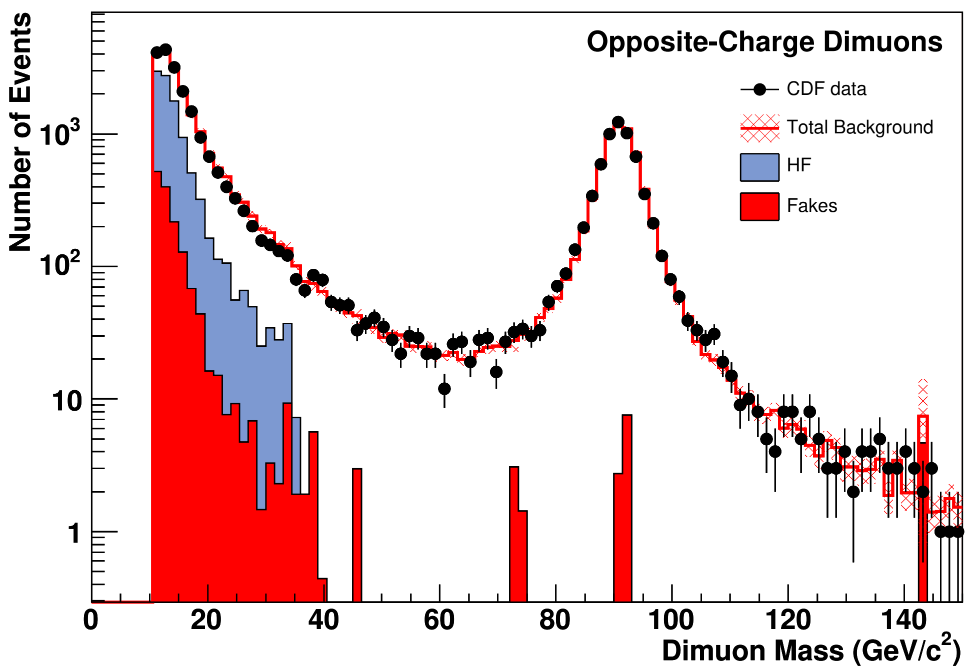

Figure 3: Fit of HF+DY+fakes dimuon mass distribution to the observed data for opposite-charge dimuons. The HF normalization is the only free parameter of the fit. The blue (light gray) filled histogram is the HF and the red (dark gray) is the fakes. The thick line represents the total background, which is almost exclusively DY, HF, and fakes at the opposite-charge dimuon level. The hatched areas indicate the total uncertainty on the prediction.

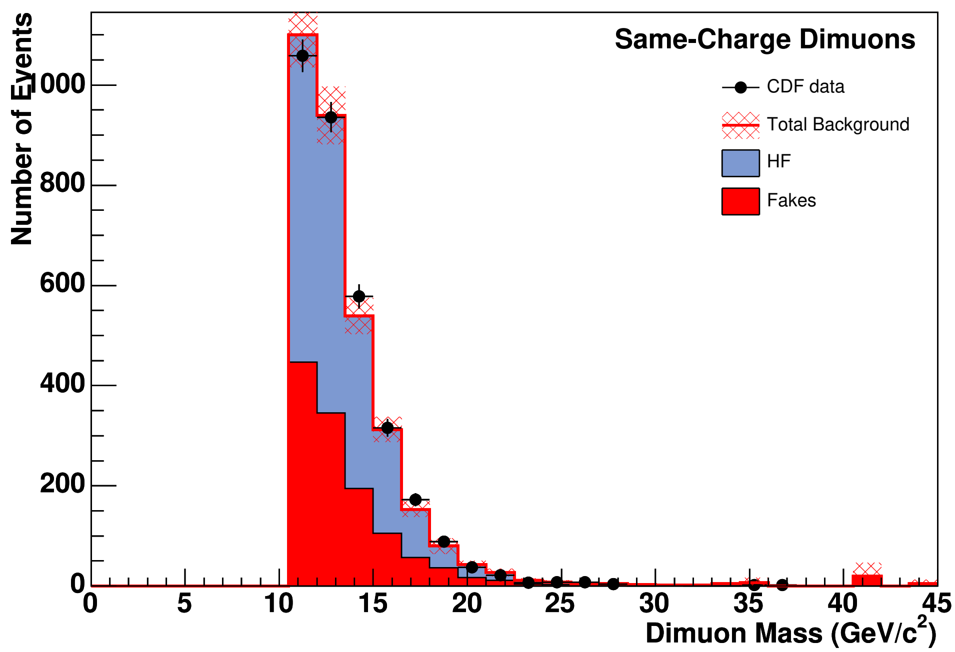

Figure 4: Fit of HF+DY+fakes dimuon mass distribution to the observed data for same-charge dimuons. The HF normalization is the only free parameter of the fit. The blue (light gray) filled histogram is the HF and the red (dark gray) is the fakes.Blue (light gray) is the HF, red (dark gray) is the fakes. The thick line represents the total background, which is almost exclusively HF and fakes at the same-charge dimuon level. The hatched areas indicate the total uncertainty on the prediction.

significance ($|d_0|/\delta|d_0| > 5$). These cuts favor HF events but reduce our HFR dataset statistics. The HF-estimation method systematic uncertainty is about 25% in the signal region.

Although the HF normalization is extracted from the inclusive analysis sample, with dimuon mass greater than 10.5 GeV/c^2 (to avoid the Υ resonance) and no additional $\not\!\!E_T$ or jet multiplicity requirements, the agreement of our HF predictions in both event yields and kinematic distributions for all our dimuon and trilepton control regions is excellent, as we show in Section 7.

4.2 MC-estimated Backgrounds

We use the PYTHIA [26] generator to model the DY, WW, ZZ, and $t\bar{t}$ background, and MADEVENT [27] for the WZ background [28]. The DY background includes the decay to tau leptons with subsequently decays to muons. We use the CTEQ5L [29] parton distribution functions (PDF) throughout. For the trilepton predictions we require the reconstructed electrons and muons to be kinematically matched with the generator-level leptons, in order not to double-count some of the fake-lepton contribution. To estimate the trilepton background from DY+γ, we relax this matching requirement, demand that the electron is identified at the event-generator level as a photon-conversion product, and normalize the unique surviving event using a scale factor [25]. This scale factor accounts for the difference in conversions-removal inefficiency between the observed data and the MC simulation. In the remainder of the paper we add the DY+γ background to the rest of the diboson contribution (WW, ZZ, and WZ). We process each generated event with the CDF detector simulation, based on GEANT [30]. We normalize all samples using the leading-order theoretical cross sections multiplied by the appropriate scale ("K-factor") to correct for next-to-leading order effects [31, 32]. Scale factors that correct for the known differences in lepton identification and reconstruction efficiencies between the observed data and the MC simulation are also applied.

5 SUSY Signal Scenarios

This analysis is a generic search for trilepton events in which we focus on minimizing the SM background. We nevertheless consider two mSUGRA [33] SUSY signal scenarios, defined by the value of the common sfermion mass (m_0) and common gaugino mass ($m_{\frac{1}{2}}$) at unification scale, the trilinear coupling (A_0), the ratio of the two Higgs fields vacuum expectation values ($\tan\beta$), and the sign of the higgsino mixing parameter ($\mathrm{sign}(\mu)$):

- SIG1: m_0=100 GeV/c^2, $m_{\frac{1}{2}}$=180 GeV/c^2, A_0=0, $\tan\beta$=5, $\mu > 0$. The expected cross section times the branching ratio ($\mathcal{B}$) to leptons is $\sigma \times \mathcal{B} = 0.642 \times 0.22$ pb. The cross section was obtained using the next-to-leading order calculation of PROSPINO [34] and the branching ratio using PYTHIA. The corresponding chargino and lightest neutralino masses would be 116 GeV/c^2 and 65 GeV/c^2, respectively.

- SIG2: m_0=74 GeV/c^2, $m_{\frac{1}{2}}$=168 GeV/c^2, A_0=0, $\tan\beta$=3, $\mu > 0$. The expected cross section times the branching ratio to leptons is $\sigma \times \mathcal{B} = 1.023 \times 0.5$ pb, as given by PROSPINO and PYTHIA. The corresponding chargino and lightest neutralino masses would be 103 GeV/c^2 and 57 GeV/c^2, respectively.

These two signal scenarios serve as benchmarks of possible SUSY signal and were used for the Signal/$\sqrt{\text{Background}}$ optimization of the minimum $\not\!\!E_T$ requirement at the signal region, which is set at 15 GeV. The mass spectrum of the supersymmetric particles was obtained with ISAJET [35] and the events are generated with PYTHIA. The SIG1 scenario leads to three-body decays (Fig. 2a) of the lightest chargino ($\tilde{\chi}_1^{\pm}$)

and the next-to-lightest neutralino ($\tilde{\chi}_2^0$) with branching ratios to electrons and muons suppressed, due to the low branching ratio of the gauge bosons to leptons. On the other hand, the SIG2 scenario leads exclusively to two-body decays (Fig. 1a) of both gauginos to sleptons, with $\tilde{\chi}_1^\pm$ decaying always to a final-state tau (produced from a stau decay). Our analysis is more sensitive to SIG2, due to the higher cross section and our ability to select events with low momentum final-state leptons, originating from tau decays.

6 Systematic Uncertainties

The significance of any potential new-physics signal is correlated to our overall background estimation uncertainty. Because we perform a counting experiment, we concentrate on the uncertainties on the expected number of background and signal events. The event-yield systematic uncertainty is naturally different for MC-simulated and CDF-data-estimated physical processes. We first discuss the systematic uncertainty on the MC-estimated backgrounds and SUSY signals and then we treat the systematic uncertainty on the CDF-data-based background of HF and fake leptons.

The sources of systematic uncertainty in the signal region, with their effect on signal and MC-estimated background event yields are:

- the luminosity uncertainty (6%) [36],
- the lepton-identification scale factors uncertainty ($\sim 10\%$),
- the trigger efficiency uncertainty ($\sim 1\%$),
- the jet-energy scale uncertainty ($\sim 1\%$) [24]; this source of systematic uncertainty is responsible for migrating events from one control or signal region to another,

since variations in jet energies affect both the corrections to the $\not\!\!E_T$ and the jet multiplicity,

- the PDF uncertainty (1%-2%) [37].

- the cross sections theoretical uncertainty (5-12% depending on the process) [31, 32],

- the uncertainty on the initial- and final-state QCD-induced radiation (ISR/FSR) [38], which has an effect of 4% and 12% for background and signal MC samples, respectively, and

- the uncertainty induced from the limited MC statistics: for the SIG2 MC it is $\sim$ 2% for the dimuons and $\sim$ 6% for the trileptons; for the standard model background MC it is $\sim$ 3% for the dimuons and $\sim$ 40% for the trileptons (the latter mainly due to the DY+γ limited MC statistics).

All the above systematic uncertainties are correlated among the different physics processes (DY, diboson, $t\bar{t}$), with the exception of the cross section systematic uncertainty and MC samples statistics. The sources of systematic uncertainties are considered uncorrelated with each other and the respective uncertainties are summed in quadrature with each other to give the total yield uncertainties in the control and signal regions.

The HF-estimation systematic uncertainty consists of a part that is anti-correlated with the DY+fakes systematic uncertainty (because the HF weights are given by the fit of the DY+fakes+HF to the observed data, and a varied level of DY+fakes affects these weights) and an uncorrelated part (from the fit uncertainty of about 2-4% for the fixed DY+fakes level and from the HF-estimation method systematic uncertainty, as described in Section 4.1.2). The correlated DY+HF+fakes systematic uncertainty

Table 1: The dimuon and trilepton event-yield systematic uncertainties for the backgrounds in the signal region. The uncertainties are summed based on the contributions of the separate backgrounds. The upper part of the table shows the MC-related systematic uncertainties whereas the lower part shows the systematic uncertainties for the CDF-data-estimated backgrounds. The uncertainties due to the MC statistics are not shown.

Source	Dimuons	Trileptons
Electron scale factors	$\pm 0\%$	$\pm 2\%$
Muon scale factors	$\pm 8\%$	$\pm 5\%$
Luminosity	$\pm 3\%$	$\pm 2\%$
Trigger efficiency	$\pm 0.5\%$	$\pm 0.2\%$
PDF	$\pm 2\%$	$\pm 1\%$
ISR/FSR	$\pm 2\%$	$\pm 1\%$
Theoretical cross sections	$\pm 3\%$	$\pm 2\%$
Jet-energy scale	$\pm 0.5\%$	$\pm 0.02\%$
Total MC syst.	$\pm 9\%$	$\pm 6\%$
Fakes estimation	$\pm 8\%$	$\pm 25\%$
HF estimation	$\pm 5\%$	$\pm 2\%$
Total (with correlations)	$\pm 10\%$	$\pm 24\%$

is about 22%. The fake-lepton uncertainty is set to a conservative maximum-envelope 50% level, which is determined by studying different jet-triggered samples [25].

For the total systematic uncertainty of the predicted SM event yield in all control regions we take into account all correlations among physics processes. For each source of systematic uncertainty affecting the MC samples, we vary all MC samples (including DY) in a correlated manner and redo the fit of DY+fakes+HF to the observed data to extract a new HF estimation. The total variation gives us the total effect of the systematic uncertainty. The same procedure is followed when we include the fake-lepton estimation uncertainty and its effect on HF due to the above fit.

The effect of the systematic uncertainties on the background and SUSY signal expected event yields in the signal region can be found in Tables 1 and 2 respectively.

Table 2: The dimuon and trilepton event-yield systematic uncertainties for the SIG2 SUSY signal in the signal region. The systematic uncertainties for the SIG1 SUSY signal are identical.

Source	Dimuons	Trileptons
Electron scale factors	$\pm 0\%$	$\pm 6\%$
Muon scale factors	$\pm 11\%$	$\pm 15\%$
Luminosity	$\pm 6\%$	$\pm 6\%$
Trigger efficiency	$\pm 0.9\%$	$\pm 0.5\%$
PDF	$\pm 1\%$	$\pm 1\%$
ISR	$\pm 12\%$	$\pm 12\%$
Theoretical cross sections	$\pm 10\%$	$\pm 10\%$
Jet-energy scale	$\pm 0.3\%$	$\pm 0.6\%$
MC statistics	$\pm 2\%$	$\pm 6\%$
Total	$\pm 20\%$	$\pm 24\%$

7 Control Regions

We investigate control regions defined by the dimuon mass, $\not\!\!E_T$ and jet multiplicity, as shown in Fig. 5. Overall, 22 dimuon and trilepton control regions are defined. Most control regions we investigate are naturally SM-dominated with little expectation of SUSY signal. Low $\not\!\!E_T$ and $M_{\mu\mu}$ regions are dominated by the HF background, whereas the $76 < M_{\mu\mu} < 106$ GeV/c^2 region is almost exclusively populated with Z bosons.

The 5 GeV gap in the $\not\!\!E_T$ cuts between the signal and the control regions ensures that the low $\not\!\!E_T$ control regions contain a negligible amount of signal. We compare the SM event-yield predictions with observed events in the control regions (along with kinematic plots) before looking at the signal region. We present here a Z boson resonance control region, a low $\not\!\!E_T$ control region and three control regions that result from the inversion of one of the three signal region requirements at a time [dimuon mass ($M_{\mu\mu}$), or $\not\!\!E_T$, or jet multiplicity (N_{jet})]. In region Z, we require that the muons have opposite charge, and that the dimuon mass lie between 76 and 106 GeV/c^2. We use this control region for validating the luminosity, the trigger efficiencies, and muon-identification scale factors. In region A, we require that $\not\!\!E_T < 10$ GeV and $M_{\mu\mu} > 10.5$ GeV/c^2.

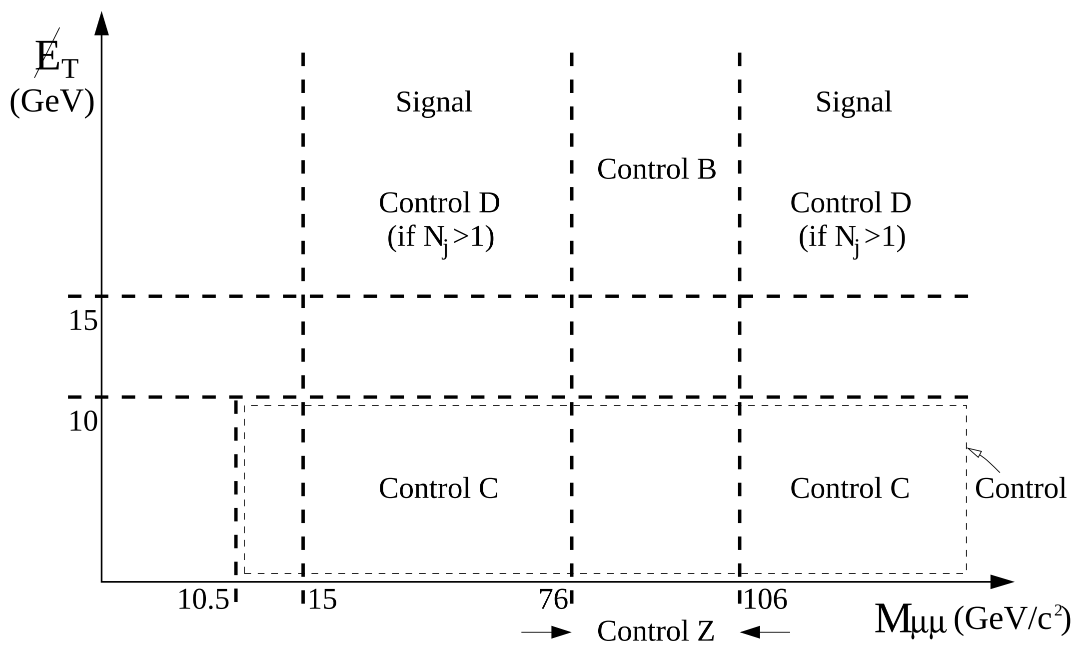

Figure 5: The control and signal regions used in our analysis are defined in the dimuon mass vs. $\not\!\!E_T$ plane, with the extra requirement of low (≤ 1) or high (> 1) jet multiplicity. In this paper we show results for the control regions that result from the inversion of one of the three main kinematic selections (dimuon mass, missing transverse energy, and jet multiplicity), with the addition of a Z-mass control region (Control Z) and a low-$\not\!\!E_T$ inclusive control region (Control A). The control regions above are defined for low jet multiplicity, unless otherwise stated.

Table 3: Expected and observed dimuon event yields, in all control regions and the signal region. The expected SUSY signal event yield is for the SIG2 mSUGRA scenario. Combined statistical and systematic uncertainties are shown. The signal region without a requirement for a third lepton is a dimuon control region.

Region	DY	HF	Fakes	Diboson	$t\bar{t}$	**Total SM expected**	**SUSY expected**	**Observed**
Control Z	6419 ± 709	-	10 ± 11	2.4 ± 0.2	1.18 ± 0.14	6433 ± 712	0.30 ± 0.07	6347
Control A	14820 ± 2242	9344 ± 1612	2294 ± 1148	1.03 ± 0.09	0.12 ± 0.03	26459 ± 1429	0.9 ± 0.2	26295
Control B	217 ± 25	-	9 ± 7	1.7 ± 0.2	0.27 ± 0.05	227 ± 26	0.5 ± 0.1	253
Control C	5770 ± 1043	2238 ± 384	466 ± 234	0.49 ± 0.07	0.02 ± 0.01	8474 ± 857	0.7 ± 0.2	8205
Control D	7.8 ± 1.5	9 ± 4	0.3 ± 0.3	0.21 ± 0.07	4.1 ± 0.4	22 ± 5	1.8 ± 0.4	23
Signal Reg.	169 ± 30	90 ± 20	49 ± 25	6.5 ± 0.4	0.96 ± 0.11	315 ± 37	17 ± 3	297

This region is used for verifying our knowledge of HF and fake-lepton backgrounds. In region B, we require $\not{E}_T > 15$ GeV, dimuon mass within the Z-mass region and low jet multiplicity. This region helps us verify our background prediction in a low-yield region as most Z events are characterized by low $\not{E}_T$. In region C, we require $\not{E}_T < 10$ GeV, exclusion of the Z mass region, $M_{\mu\mu} > 15$ GeV/c^2, and low jet multiplicity (at most one jet). This region along with region A are the ones with the highest population of HF events. In region D, we require $\not{E}_T > 15$ GeV, exclusion of the Z mass region, $M_{\mu\mu} > 15$ GeV/c^2, and high jet multiplicity (more than one jet). This region is expected to be the most sensitive to $t\bar{t}$ production. We finally study the dimuon events with all signal-region kinematic cuts applied, but before the requirement for a third lepton. This is a critical control region as the trilepton signal is a subset of this region. Table 3 shows the expected and observed number of dimuon events in our control regions, and Table 4 shows the expected and observed number of trilepton events. After requiring the presence of a third electron or muon, only control regions Z, A and C are populated with experimental data. Region Z trilepton event yields establish our understanding of the electron fakes, since the third electron in Z boson decays comes almost exclusively from hadronic activity. On the other hand, trilepton regions Z and C confirm our understanding of the HF and fake backgrounds for trileptons.

Figs. 6 and 7 show the dimuon mass and $\not{E}_T$ distributions for the dimuon control regions. The agreement between observed data and prediction in the control regions is

Table 4: Expected and observed trilepton event yields, in all control regions and the signal region. The expected SUSY signal event yield is for the SIG2 mSUGRA scenario. Combined statistical and systematic uncertainties are shown.

Region	DY	HF	Fakes	Diboson	$t\bar{t}$	**Total SM expected**	**SUSY expected**	**Observed**
Control Z	0.2 ± 0.2	-	2.5 ± 1.2	0.26 ± 0.06	-	3 ± 1	0.06 ± 0.01	4
Control A	0.3 ± 0.2	6 ± 3	7.6 ± 3.8	0.25 ± 0.08	-	14 ± 4	0.08 ± 0.02	16
Control B	-	-	0.2 ± 0.1	0.094 ± 0.009	-	0.3 ± 0.1	0.10 ± 0.03	0
Control C	0.2 ± 0.2	3 ± 2	2 ± 1	0.10 ± 0.06	-	5 ± 2	0.06 ± 0.02	8
Control D	-	-	0.02 ± 0.01	0.003 ± 0.002	0.011 ± 0.008	0.03 ± 0.01	0.04 ± 0.02	0
Signal Reg.	**-**	**0.06 ± 0.04**	**0.2 ± 0.1**	**0.15 ± 0.06**	**-**	**0.4 ± 0.1**	**1.7 ± 0.4**	**1**

satisfactory, both in event yields and kinematic distributions.

8 Signal Region Result

After observing satisfactory agreement between experimental data and SM predictions in both the dimuon and trilepton control regions, we look at the CDF data in the trilepton signal region. We observe one event consisting of three muons. The event is characterized by low track activity and three well-identified muons that are produced within ~ 40 degrees in ϕ. Two of the muons are energetic, with transverse momenta of 45 and 21 GeV/c, and the third one is a soft muon with p_T of 8 GeV/c. Table 5 shows the main properties of this event. The event also includes one hadronic jet and two energy clusters of mostly electromagnetic energy with transverse energy of ~ 41, ~ 9, and ~ 4 GeV respectively. The jet and the muons originate from the same and only high-quality primary vertex. If the electromagnetic energy clusters correspong to real photons, the event would also be interesting in the gauge-mediated supersymmetry breaking (GMSB [39]) scenario, where the lightest neutralino decays to a photon and a gravitino, which is the LSP. In that case, the final leptonic signature of the chargino-neutralino production would be three leptons, two photons and $\not\!\!E_T$.

Figs. 9 and 10 show the transverse and lego detector displays, respectively. Fig. 8 shows some of the kinematic distributions for our trimuon event, including the three-dimensional openning angle between the leading muons, $\Delta\varphi$. The Poisson probability

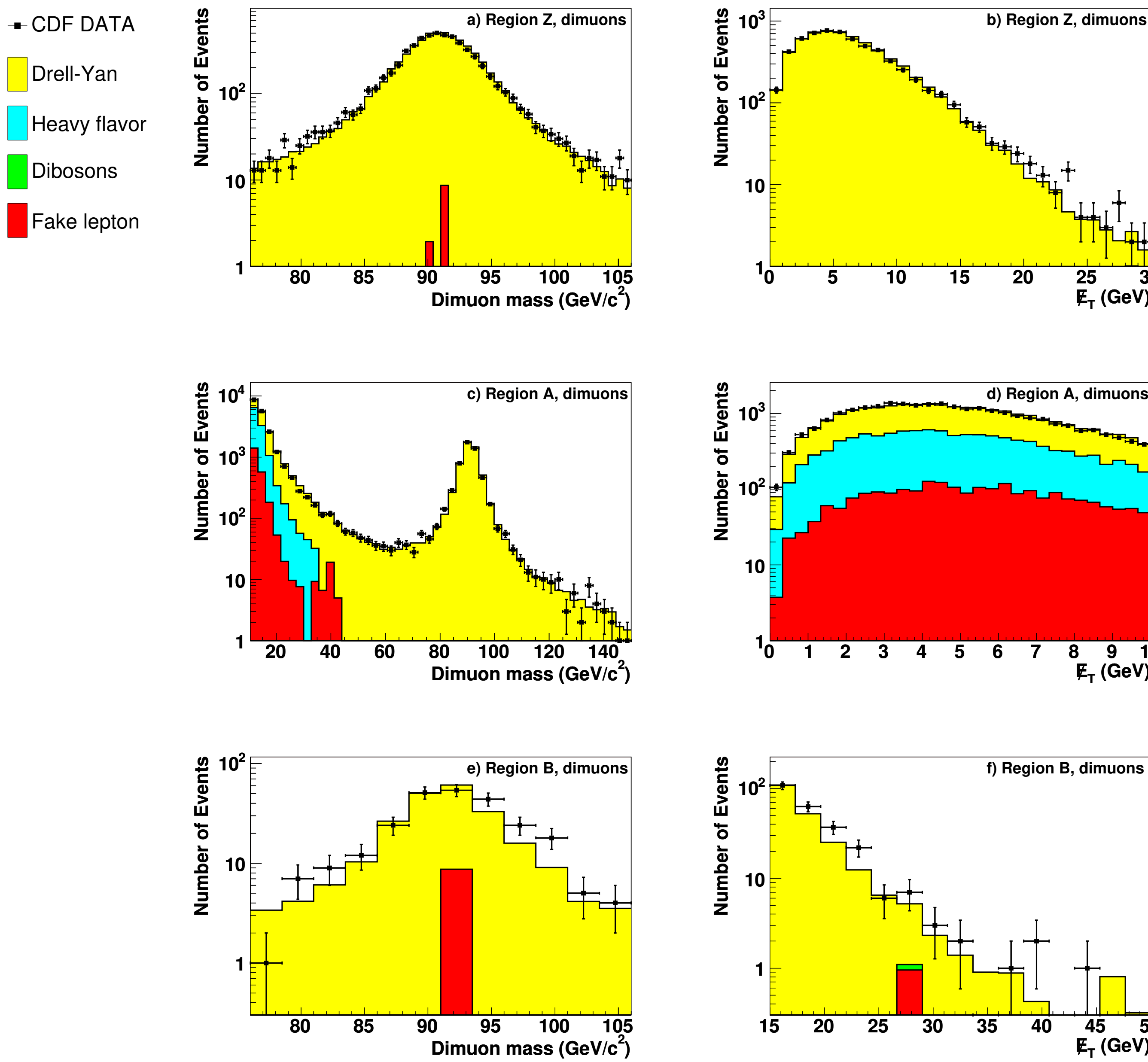

Figure 6: Dimuon mass and $\not\!\!E_T$ distributions for the SM background in the dimuon control regions Z (a,b), A (c,d), and B (e,f). The background histograms are stacked atop one another. The CDF data are indicated by points with error bars.

to see one event or more, when we expect 0.4 ± 0.1, is 32.6%.

It is interesting also to interpret this event in the context of a search only for trimuon events. The diboson backgrounds remain, but the large source of fakes in the dimuon+e sample is reduced. The total trimuon background estimation is 0.16 ± 0.04 events. The

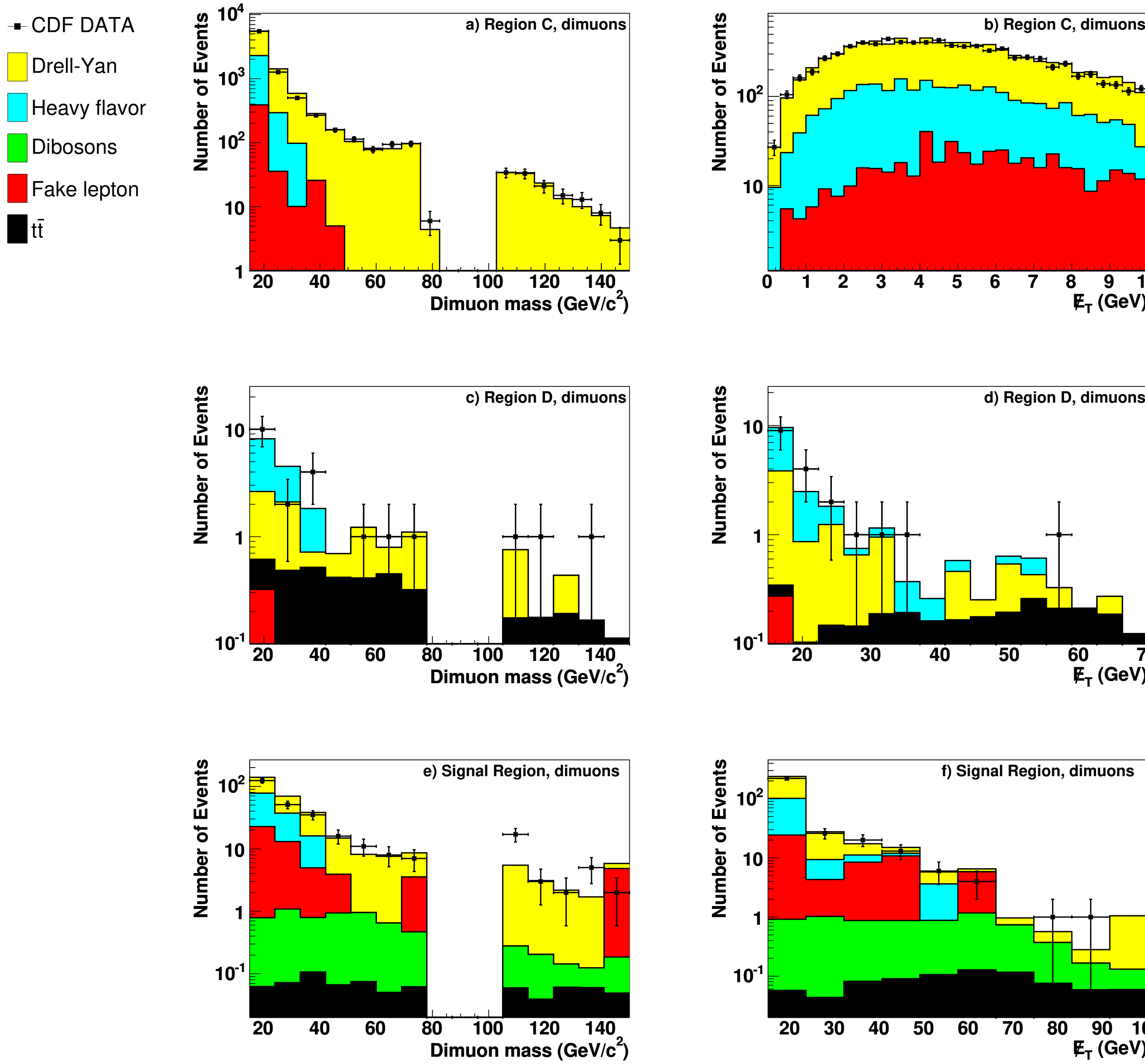

Figure 7: Dimuon mass and $\not\!\!E_T$ for the SM background in the dimuon control regions C (a,b), D (c,d), and dimuon signal region (e,f). The background histograms are stacked atop one another. The CDF data are indicated by points with error bars.

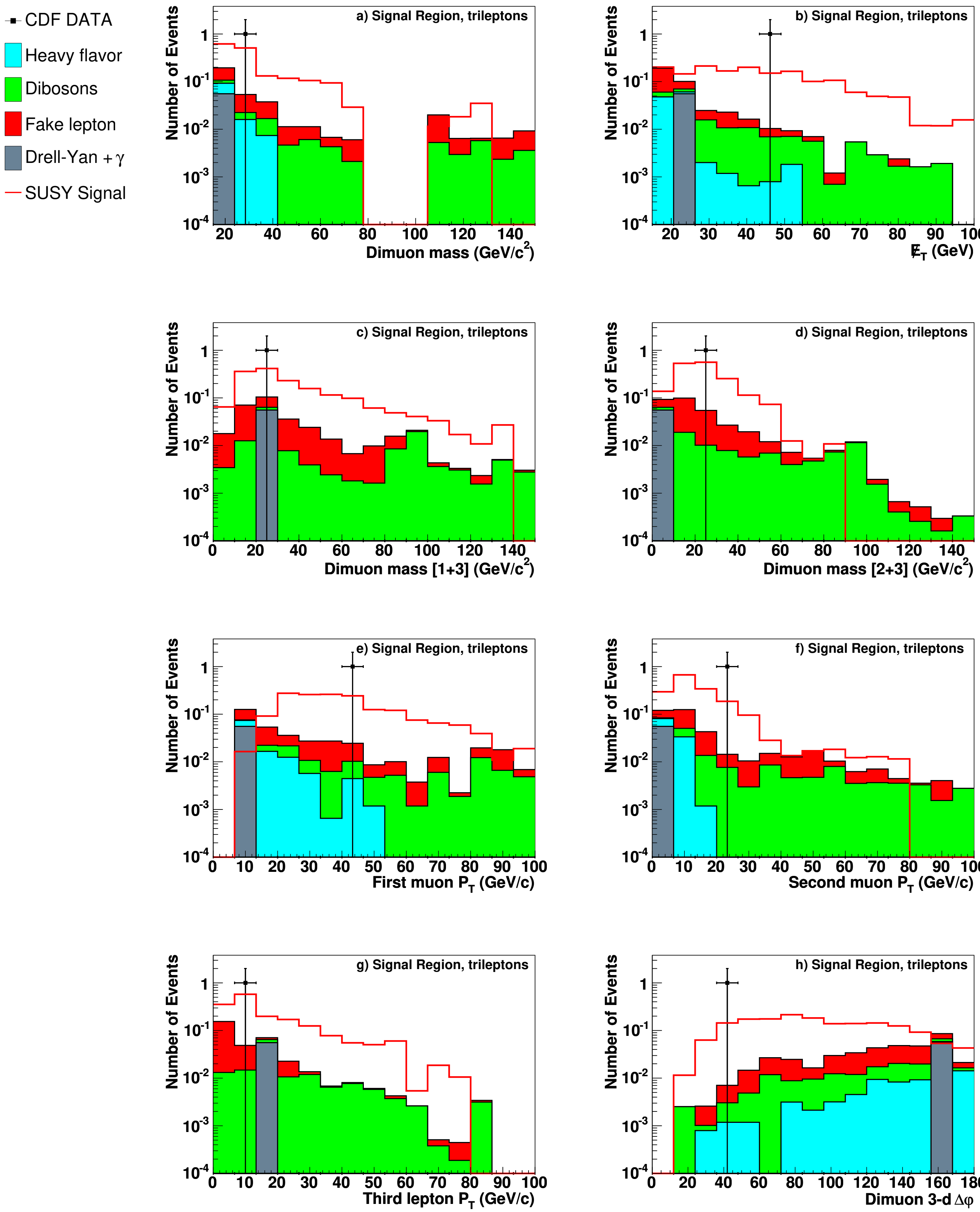

Figure 8: Kinematic variable for the SM background and the SIG2 SUSY signal, in the trilepton signal region. The background histograms are stacked atop one another; the signal histogram is not. The CDF data are indicated by points with error bars.

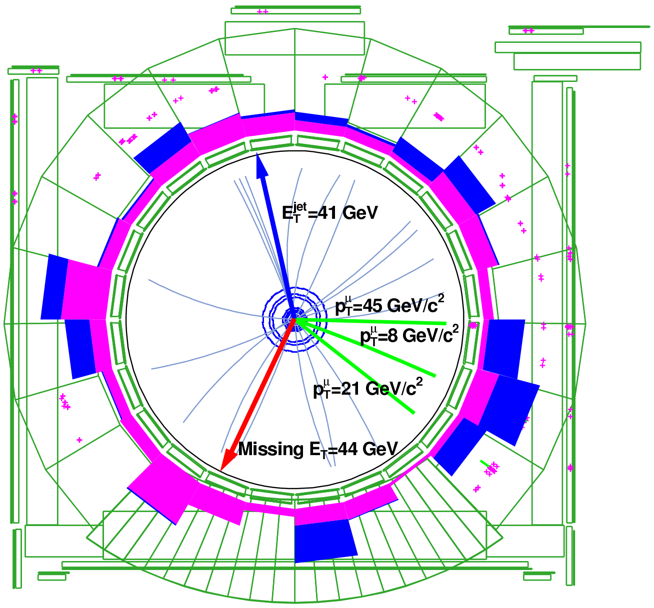

Figure 9: The trimuon event in the transverse view of the central CDF detector. Tracks with transverse momenta above 1 GeV/c and calorimeter energies above 1 GeV are shown.

Table 5: Observed trimuon event properties.

Kind of muons	CMUP - CMX - CMX
p_T of muons (GeV/c)	45.0, 21.1, 7.8
η of muons	-0.2, -0.9, 0.8
ϕ of muons (deg.)	359, 321, 340
Isolation of muons (GeV)	0.05*$p_T c$, 0.009*$p_T c$, 0.13
Charge of muons	-1, 1, -1
Dimuon masses (GeV/c^2)	29.3(1&2), 21.7(1&3), 25.7(2&3)
Transverse mass (muon+$\not\!\!E_T$)	86.4, 51.4, 34.2
3-d $\Delta\varphi$(leading muons) (deg.)	46.3
$\not\!\!E_T$(GeV)	43.8
$\not\!\!E_T$ ϕ (deg.)	205.6
Number of Jets	1
E_T of jet (GeV)	41.1
η of jet	-1.6
ϕ of jet (deg.)	102.9

Poisson probability to observe one event or more, when we expect 0.16$\pm$0.04, is 14.7%. We conclude that our event yield is consistent with the SM prediction, noting that most of the kinematics of the event - especially the angular distribution of the leptons - are not inconsistent with new physics expectation, as can be seen in Fig. 8.

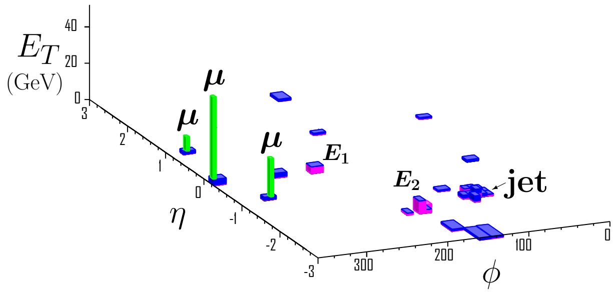

Figure 10: The trimuon event in the $\eta - \phi$ view. The calorimeter transverse energies above 1 GeV are shown. The longer bars correspond to the track momenta of the three muons (high ϕ). The calorimeter energy depositions E_1 and E_2 are mainly electromagnetic and could be associated with two photons.

We have combined the results of this analysis with other CDF trilepton analyses to set exclusion limits in several models. For mSUGRA with no slepton mixing we set a lower limit for the chargino of 129 GeV/c^2, which corresponds to an upper limit in the $\sigma \times \mathcal{B}$ of about 0.25 pb at 95% confidence level [20].

9 Acknowledgments

We thank the Fermilab staff and the technical staffs of the participating institutions for their vital contributions. This work was supported by the U.S. Department of Energy and National Science Foundation; the Italian Istituto Nazionale di Fisica Nucleare; the Ministry of Education, Culture, Sports, Science and Technology of Japan; the Natural Sciences and Engineering Research Council of Canada; the National Science Council of the Republic of China; the Swiss National Science Foundation; the A.P. Sloan Foundation; the Bundesministerium für Bildung und Forschung, Germany; the Korean Science and Engineering Foundation and the Korean Research Foundation; the Science and Technology Facilities Council and the Royal Society, UK; the Institut National de Physique Nucleaire et Physique des Particules/CNRS; the Russian Foundation for Basic Research; the Ministerio de Ciencia e Innovación, Spain; the Slovak R&D Agency;

and the Academy of Finland.

References

[1] G. Hinshaw et al. (WMAP Collaboration), `arXiv:0803.0732[astro-ph]`.

[2] H. Baer and X. Tata, *Weak Scale Supersymmetry* (Cambridge University Press, 2006).

[3] J. Wess and B. Zumino, Phys. Lett. **B49**, 52 (1974), `arXiv:hep-ph/9906298`.

[4] Chargino-neutralino production cross-sections times branching ratios to leptons of the order of 0.1 fb have not been excluded yet.

[5] The R-parity is defined as $(-1)^{3(B-L)+2S}$, where B is the baryon number, L is the lepton number and S is the spin of the particle.

[6] J. Ellis, J. Hagelin, D. Nanopoulos, K. Olive, and M. Srednicki, Nucl. Phys. **B238**, 453 (1984).

[7] H. Goldberg, Phys. Rev. Lett. **50**, 1419 (1983).

[8] E. Witten, Nucl. Phys. **B188**, 513 (1981).

[9] N. Sakai, Z. Phys. C **11**, 153 (1981).

[10] S. Dimopoulos, Nucl. Phys. **B193**, 150 (1981).

[11] S. Dimopoulos, S. Raby, and F. Wilczek, Phys. Rev. D **24**, 1681 (1981).

[12] H. Baer and X. Tata, Phys. Lett. **B155**, 278 (1986).

[13] H. Baer, H. Hagiwara, and X. Tata, Phys. Rev. D **35**, 1598 (1987).

[14] H. Baer and X. Tata, Phys. Rev. D **47**, 2739 (1993).

[15] H. Baer, C. Kao, and X. Tata, Phys. Rev. D **48**, 5175 (1993).

[16] J. Lopez, D. Nanopoulos, X. Wang, and A. Zichichi, Phys. Rev. D **48**, 2062 (1993).

[17] M. Berggren et al. (LEP Supersymmetry Working Group) (2004), URL `http://lepsusy.web.cern.ch/lepsusy/www/sleptons_summer04/slep_final.html`.

[18] F. Abe et al. (CDF Collaboration), Phys. Rev. Lett. **80**, 5275 (1998).

[19] V. Abazov et al. (D0 Collaboration), Phys. Rev. Lett. **95**, 151805 (2005).

[20] T. Aaltonen et al. (CDF Collaboration), Phys. Rev. Lett. **99**, 191806 (2007a).

[21] D. Acosta et al. (CDF Collaboration), Phys. Rev. D **71**, 032001 (2005a).

[22] R. Downing et al., Nucl. Instrum. Methods **A570**, 36 (2007).

[23] D. Acosta et al. (CDF Collaboration), Phys. Rev. D **71**, 052003 (2005b).

[24] A. Bhatti et al., Nucl. Instrum. Methods **A566**, 375 (2006).

[25] T. Aaltonen et al. (CDF Collaboration) (2007b), submitted to Phys. Rev. D, `arXiv:0711.3161[hep-ex]`.

[26] T. Sjöstrand, S. Mrenna, and P. Skands, JHEP05(2006)026 (2006), PYTHIA 6.4, `arXiv:hep-ph/0603175`.

[27] F. Maltoni and T. Stelzer, JHEP02(2003)027 (2003), `arXiv:hep-ph/0208156`.

[28] PYTHIA does not include the $W\gamma$ diagrams when it generates WZ.

[29] H. Lai et al. (CTEQ Collaboration), Eur. Phys. J. C **12, 375** (2000a).

[30] R. Brun, R. Hagelberg, M. Hansroul, and J. Lasalle (1978), CERN report CERN-DD-78-2-REV.

[31] J. M. Campbell and R. K. Ellis, Phys. Rev. D **60**, 113006 (1999).

[32] R. Bonciani, S. Catani, M. L. Mangano, and P. Nason, Nucl. Phys. **B529**, 424 (1998).

[33] A. H. Chamseddine, R. Arnowitt, and P. Nath, Phys. Rev. Lett. **49**, 970 (1982).

[34] W. Beenakker et al., Phys. Rev. Lett. **83**, 3780 (1999), `arXiv:hep-ph/9906298`.

[35] H. Baer, F. Paige, S. Protopopescu, and X. Tata (2000), `arXiv:hep-ph/0001086`.

[36] S. Klimenko, J. Konigsberg, and T. M. Liss (2003), FERMILAB-FN-0741.

[37] H. L. Lai et al., Eur. Phys. J. C **12**, 375 (2000b).

[38] A. Abulencia et al. (CDF Collaboration), Phys. Rev. D **73**, 112006 (2006).

[39] G. F. Giudice and R. Rattazzi, Phys. Rept. **322**, 419 (1999).